





**Stopping power of water for carbon ions with energies in the Bragg peak region**

W. Y. Baek , T. Braunroth, L. de La Fuente Rosales , J. M. Rahm , and H. Rabus   
*Physikalisch-Technische Bundesanstalt, Bundesallee 100, 38116 Braunschweig, Germany*



(Received 14 October 2020; accepted 1 December 2020; published 18 December 2020)

The stopping power of liquid water was measured for carbon ions with energies in the Bragg peak region using the inverted Doppler shift attenuation method. Among the semiempirical data, the results of this work agree best with the data recommended in the Errata and Addendum of ICRU Report No. 73, which is based on an  $I$  value of 78 eV for water. The agreement was worse when the present results were compared to the newer recommendation of the ICRU published in ICRU Report No. 90. The SRIM code seems to slightly overestimate the stopping power of water for carbon ions above 3 MeV. A semiexperimental stopping power of water for  $\alpha$  particles was derived from the present results using the theoretical ratio between the stopping powers of water for carbon ions and  $\alpha$  particles computed by means of the CASP code. These values agree well with the experimental data for  $\alpha$  particles within the uncertainties.

DOI: [10.1103/PhysRevE.102.062418](https://doi.org/10.1103/PhysRevE.102.062418)

**I. INTRODUCTION**

The number of radiotherapy facilities using protons and heavier ions is growing steadily. The main advantage of the use of ion beams over photon radiation from a physical point of view is the inverse depth dose profile with a sharp dose escalation at the end of the ion range, called the Bragg peak. This allows us to deposit the major part of the ion kinetic energy in the target volume while sparing surrounding normal tissues from an unwanted dose. In order to fully exploit the advantage of ion beam therapy, the effective range and stopping power of tissue for ions must be accurately known. Moreover, the biological effectiveness of a radiation varies with the linear energy transfer (LET) or the stopping power. The knowledge of the stopping power of tissue is therefore required to assess not only the amount of physical energy deposition but also the biologically effective dose. In this context, the ion stopping power of liquid water is of great importance as it makes up more than 60% of human tissue.

Apart from the relevance for medical applications, the ion stopping power near its maximum is also of interest for elucidating the interaction of charged particles with matter. In this intermediate energy region, the speed of ions is comparable to that of target valence electrons so that the energy loss mechanisms of ions are increased in their complexity. Here, the ion stopping power depends sensitively on the physical state of the target.

Since the first measurement [1] of  $\alpha$ -particle ranges in liquid water in the 1920s, a number of experimental studies on the ion stopping power of liquid water have been made. In the energy region around the stopping power maximum, most of these studies were performed using  $\alpha$  particles emitted from radioactive sources [2–7]. For protons, measurement in the intermediate energy region was reported by Shimizu *et al.* [8], who determined the energy loss of 2 MeV-protons in a liquid water jet of 50  $\mu\text{m}$  in diameter. In subsequent work,

they extended the measurement for proton energies down to 0.3 MeV [9]. One year later, Siiskonen *et al.* [10] published the stopping power of liquid water for higher proton energies ranging from 4.7 to 15.2 MeV.

For carbon ions, an experiment regarding the stopping power of liquid water in the Bragg peak area was performed by the present group [11]. The measurement, which was of preliminary nature, was done for projectile energies  $T$  from 1 to 6 MeV by employing the so-called inverted Doppler shift attenuation (IDSA) method [12]. In this method, the stopping power is extracted from the Doppler-shifted energy spectra of  $\gamma$  quanta emitted from the first  $2+$  state in  $^{12}\text{C}^*$  nuclei, whose level lifetime is known with a relatively high precision. The results of the measurement confirmed that the stopping power of liquid water for carbon ions is considerably lower than that of water vapor.

As the accuracy of the early measurement suffered much from experimental shortcomings such as a high background in the region of interest of the Doppler-shifted  $\gamma$  energy spectrum, the stopping power of liquid water for  $^{12}\text{C}$  ions was remeasured in this work by applying the same method, but with an improved experimental setup. The major improvement was achieved by the use of an anti-Compton spectrometer, which raised the signal-noise ratio in the relevant region of the  $\gamma$  energy spectrum by a factor of about 5. Furthermore, more accurate start velocity and angle distributions of excited  $^{12}\text{C}^*$  projectiles were employed in deducing the stopping power from the Doppler-shifted  $\gamma$  energy spectrum.

**II. MEASUREMENT PRINCIPLE**

The IDSA method [12] used in this work has the advantage that it enables the measurement of stopping power for ions in any aggregate state. As the method was detailed in an earlier work [11], only the derivation of relevant equations is

explained in the following. In the conventional transmission experiment, the stopping power  $S$  is determined from the kinetic energy loss  $\Delta T$  of the projectile after traversing a target of known thickness  $\Delta x$ :  $S = -\Delta T/\Delta x$ . In the IDSA method,  $S$  is derived from the temporal change of the projectile velocity  $v$  using the relation  $S = -dT/dx = -mdv/dt$ , where  $m$  is the mass of the projectile.

The projectile velocity can be determined from the Doppler shift of the energy  $E_\gamma$  of  $\gamma$  quanta emitted from the projectile, which was produced in an excited nuclear state and decays during its slowing down in the target. The relation between the projectile velocity  $v$  at the moment of the emission of  $\gamma$  quanta and the shift of the  $\gamma$  energy is given by the Doppler formula

$$E_\gamma = E_0 \frac{\sqrt{1 - (v/c)^2}}{1 - (v/c)\cos\vartheta}, \quad (1)$$

where  $E_0$  is the  $\gamma$  energy in the rest frame of the projectile,  $c$  is the speed of the light, and  $\vartheta$  is the  $\gamma$  emission angle with respect to the moving direction of the projectile. In this work, carbon projectiles were produced in the first excited nuclear state with the level energy of  $E_0 = 4438.1$  keV [13] by means of the  $^{12}\text{C}(\alpha, \alpha')^{12}\text{C}^*$  reaction.

The information on the time  $t$  elapsed between the production of excited  $^{12}\text{C}^*$  projectiles and their decay emitting  $\gamma$  quanta is provided by the exponential decay law:

$$\frac{dN}{dt} = -\frac{N_0}{\tau} e^{-t/\tau}, \quad (2)$$

where  $\tau$  is the lifetime of the first excited state in  $^{12}\text{C}$  and amounts to  $60.9 \pm 3.5$  fs [13]. The counts  $d\hat{N}/dE_\gamma$  of  $\gamma$  quanta per energy in the interval  $[E_\gamma, E_\gamma + dE_\gamma]$  can be written as

$$\frac{d\hat{N}}{dE_\gamma} = \frac{dN}{dt} \times \frac{dt}{dv} \times \frac{dv}{dE_\gamma}, \quad (3)$$

where  $dN/dt$  is given by Eq. (2),  $dv/dE_\gamma$  is obtained from Eq. (1), and  $dt/dv$  is proportional to the reciprocal stopping power  $S^{-1}$ . It furthermore follows from the relation  $S = -dT/dx = -mdv/dt$  that

$$t(v) = -\int_v^{v_0} \frac{m du}{S(u)}. \quad (4)$$

The formula for the  $\gamma$  energy spectrum  $d\hat{N}/dE_\gamma$  in dependence of the stopping power  $S(v)$  can be obtained by combining Eqs. (2)–(4):

$$\frac{d\hat{N}}{dE_\gamma} = N_0 \exp\left(-\int_v^{v_0} \frac{m}{\tau S(u)} du\right) \frac{m}{\tau} \frac{1}{S(v)} \frac{dv}{dE_\gamma}. \quad (5)$$

Equation (5) can only be applied if all  $^{12}\text{C}^*$  projectiles are produced with one start velocity  $v_0$ . In the laboratory frame, however,  $^{12}\text{C}^*$  nuclei are produced with diverse start velocities so that the measured  $\gamma$  energy spectrum  $dN_a/dE_\gamma$  is a superposition of the spectra originating from  $^{12}\text{C}^*$  projectiles with different start velocities:

$$\frac{dN_a}{dE_\gamma} = \int \exp\left(-\int_v^{v_0} \frac{m}{\tau S(u)} du\right) \frac{m}{\tau} \frac{1}{S(v)} \frac{dv}{dE_\gamma} N_0 W(v_0) dv_0. \quad (6)$$

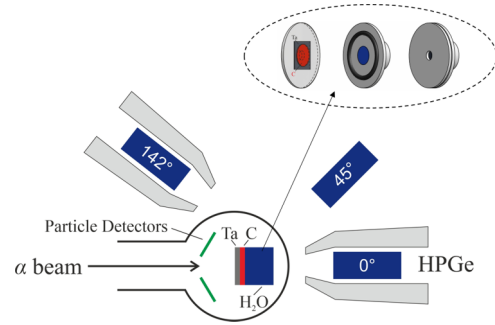


FIG. 1. Schematic view of the experimental setup and of the water target system. The gray shaded jacket represents the Pb collimator and BGO anti-Compton shield. The target system consists of two copper discs carrying a carbon coated tantalum foil with a thickness of  $5 \mu\text{m}$  and a water cavity. Both discs are screwed together with a Viton O ring in between.

In Eq. (6),  $N_0 W(v_0) dv_0$  is the number of  $^{12}\text{C}^*$  projectiles created in the velocity interval  $[v_0, v_0 + dv_0]$ . In the following, the  $\gamma$  energy spectrum  $dN_a/dE_\gamma$  is called an attenuated spectrum to indicate that it is generated by  $^{12}\text{C}^*$  projectiles with attenuating speed.

According to Eq. (6), two experiments are needed to determine the stopping power of water for  $^{12}\text{C}$  ions. Along with the energy spectrum of  $\gamma$  quanta emitted from  $^{12}\text{C}^*$  projectiles slowing down in water, the start energy distribution  $N_0 W(v_0)$  of  $^{12}\text{C}^*$  projectiles has to be measured. The latter can be determined by means of the  $\gamma$  energy spectrum  $dN_u/dE_\gamma$ , called an unattenuated spectrum in the following, which originates from  $^{12}\text{C}^*$  projectiles decaying without energy loss in vacuum. This determination is possible if the  $\gamma$  detector is placed at  $0^\circ$  with respect to the  $\alpha$  beam direction. The flight angle of  $^{12}\text{C}^*$  projectiles with respect to the  $\alpha$  beam axis is then equal to the  $\gamma$  emission angle. In this case, the flight angle  $\theta$  as well as the start velocity  $v_0$  of  $^{12}\text{C}^*$  projectiles can be deduced from the magnitude of the Doppler shift of the  $\gamma$  energy according to Eq. (1). It should be noted that  $\theta$  and  $v_0$  are related to each other in two body kinematics as is the case for the  $^{12}\text{C}(\alpha, \alpha')^{12}\text{C}^*$  reaction used in this work. It follows then for the start velocity distribution of  $^{12}\text{C}^*$  projectiles that

$$N_0 W(v_0) = \frac{dN_u}{dE_\gamma} \frac{dE_\gamma}{dv_0}, \quad (7)$$

where  $dE_\gamma/dv_0$  can be again calculated from Eq. (1).

### III. EXPERIMENT

The experiment was carried out at the Institute for Nuclear Physics of University of Cologne. Figure 1 shows a schematic diagram of the experimental setup, comprising a target system, several HPGe  $\gamma$  detectors at different angles, and Si-particle detectors in the backward direction with respect to the  $\alpha$  beam path. The  $\gamma$  detector at  $0^\circ$ , 72 mm in length, and 74 mm in diameter was equipped with a bismuth germanate (BGO) shield to suppress the Compton background.

As shown in Fig. 1, a water-filled cavity, 1 cm in diameter and 0.7 cm in height, was used as the target. The cavity,

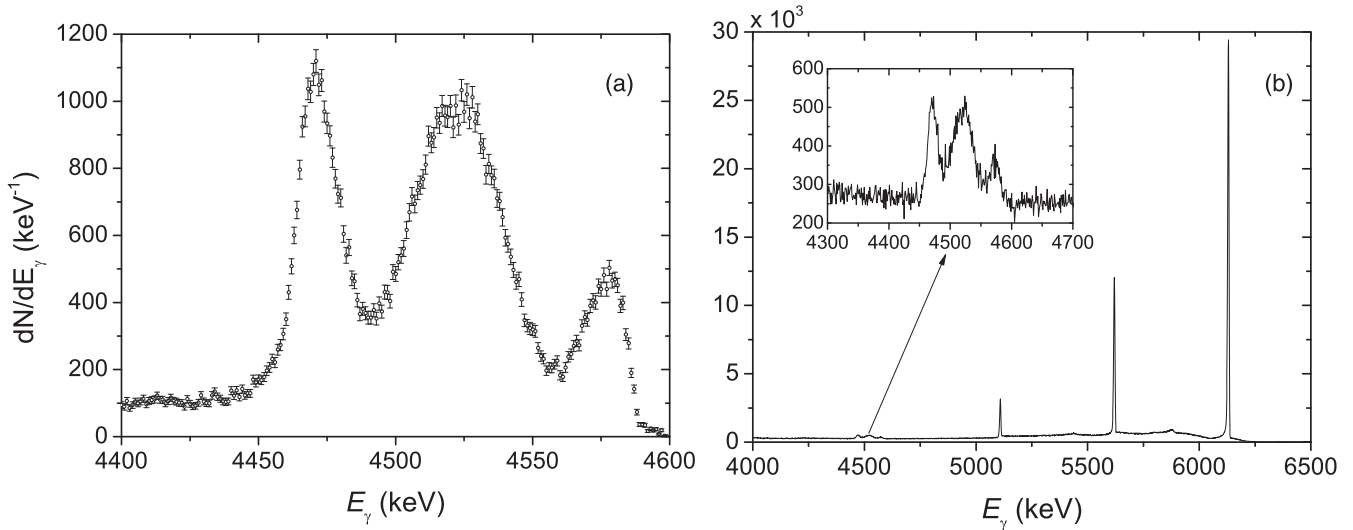


FIG. 2. Experimental unattenuated spectrum (a) and  $\gamma$  energy spectrum measured with water (b). The attenuated spectrum is displayed in the inserted box in the spectrum on the right-hand side.

milled into a copper disk, was filled fully with water and then attached to a carbon coated tantalum foil with a thickness of  $5 \mu\text{m}$ , which was glued to another copper disk with an aperture in the center. A vacuum-tight attachment was realized by screwing both copper disks together using a Viton O ring between them. The carbon coating,  $50 \text{ nm}$  in thickness, was fabricated using low-energy ion implantation by the group of H. Hofsäss at the II. Institute of Physics of University of Göttingen. The coating was water and heat resistant. No debonding of carbon from the Ta foil was observed when bombarded by  $\alpha$  particles during the measurement.

The distance between the water target and the  $\gamma$  detector at  $0^\circ$  amounted to  $16 \text{ cm}$ . A Pb cone with an opening angle of  $12.7^\circ$  was used to collimate the  $\gamma$  radiation entering the detector. The incident energy of the  $\alpha$  beam was  $12.5 \text{ MeV}$ . After traversing the Ta foil, the  $\alpha$  beam loses  $0.8 \text{ MeV}$  so that the nuclear reaction producing  $^{12}\text{C}^*$  projectiles takes place at  $11.7 \text{ MeV}$ . At this energy, the cross section of the  $^{12}\text{C}(\alpha, \alpha')^{12}\text{C}^*$  reaction was on the one hand relatively high [14] and on the other hand, the neutron production cross section was low enough to keep the neutron induced  $\gamma$  background negligibly small. The  $\alpha$  beam current amounted to typically  $8 \text{ nA}$ .

As explained above, only the  $\gamma$  energy spectrum measured at  $0^\circ$  was used to determine the stopping power of water for  $^{12}\text{C}$  ions. The  $\gamma$  energy spectra taken at other angles were used to monitor the stability of the experimental parameters such as the direction and energy of the  $\alpha$  beam since the shape of the  $\gamma$  energy spectrum sensitively depends on these parameters. An additional check of the experimental conditions was done by observing the energy of  $\alpha$  particles measured with the Si-particle detector at a backward angle.

As mentioned above, two experiments were required to determine the stopping power of water for  $^{12}\text{C}$  ions. In the first experiment, the attenuated spectrum  $dN_a/dE_\gamma$  described by Eq. (6) was measured. In this experiment,  $^{12}\text{C}^*$  projectiles were produced by an incident  $\alpha$  beam in the carbon layer coated on the Ta foil and then slowed down in the subsequent water volume. The depth of the water volume was enough

to fully stop also the  $\alpha$  beam. In the second experiment, the unattenuated spectrum  $dN_u/dE_\gamma$ , given by Eq. (7), was measured. Here, the water was removed from the water cavity so that the  $^{12}\text{C}^*$  projectiles produced in the carbon layer decayed in the vacuum without energy loss, i.e., at their initial velocity.

The energy calibration of the  $\gamma$  detector was performed by means of three  $\gamma$  lines of a  $^{226}\text{Ra}$  source at  $2204$ ,  $2293$ , and  $2447 \text{ keV}$  as well as of the  $\gamma$  line of  $^{16}\text{O}^*$  at  $6129 \text{ keV}$ , which is produced by  $\alpha$  particles impinging into water through the reaction  $^{16}\text{O}(\alpha, \alpha')^{16}\text{O}^*$ . In order to determine the energy resolution of the  $\gamma$  detector in the region of interest, i.e., at energies around  $4.438 \text{ MeV}$ , a natural copper slice was activated by means of  $18\text{-MeV}$   $\alpha$  particles, producing excited  $^{66}\text{Ga}$  nuclei. The  $\beta^+$  decay of  $^{66}\text{Ga}$  leads to  $^{66}\text{Zn}^*$ , which decays to the ground state by emitting  $\gamma$  quanta in the energy region around  $4.5 \text{ MeV}$ .

#### IV. DATA ANALYSIS

The measured  $\gamma$  energy spectra  $dN/dE_\gamma$  are represented in Figs. 2(a) and 2(b). Figure 2(a) shows the unattenuated spectrum. The  $\gamma$  energy spectrum measured with the water target is displayed in Fig. 2(b), where the  $^{16}\text{O}$  line at  $6.13 \text{ MeV}$  including the escape peaks at  $5.62$  and  $5.11 \text{ MeV}$  is clearly visible. They are produced by the excitation of  $^{16}\text{O}$  nuclei in water by the incident  $\alpha$  beam.

The attenuated spectrum originating from  $^{12}\text{C}^*$  projectiles slowing down in water is shown in the inserted box in Fig. 2(b). The background in this spectrum mainly arises from the Compton scattering of  $\gamma$  rays emitted by excited  $^{16}\text{O}^*$  nuclei. It is noteworthy that an improvement of the signal to background ratio in the attenuated spectrum by a factor of about 5 was achieved by the use of the BGO anti-Compton shield compared to the former experiment.

In the first step of the data evaluation, the measured unattenuated spectrum was deconvolved from the energy and angular resolution function of the detection system after the subtraction of the background. The background was determined from the measured data in the region above the upper

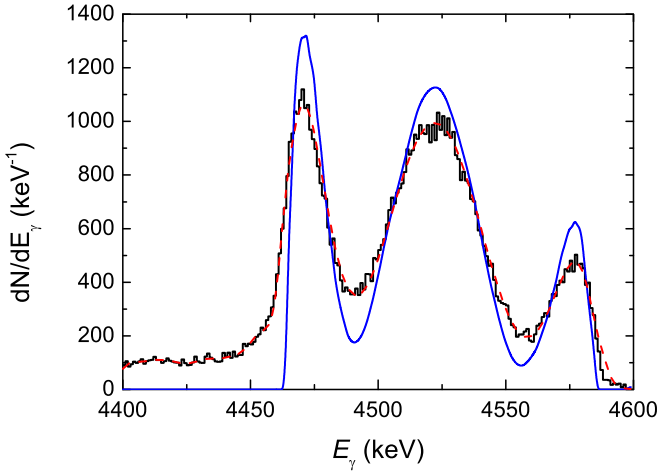


FIG. 3. Results of the deconvolution of the energy and angular resolution function from the unattenuated spectrum. The experimental spectrum ( $y_u$ ) is represented by vertical steps. The solid ( $dN_u/dE_\gamma$ ) and dashed line depict the deconvolved and refolded spectrum, respectively.

energy limit of the unattenuated spectrum. It was almost constant and nearly zero (below  $10 \text{ keV}^{-1}$ ). As mentioned above, the energy resolution function  $f(E_\gamma)$  was obtained from the  $\gamma$  line of  $^{66}\text{Zn}^*$  nuclei at an energy around 4.5 MeV. It consists of an asymmetric Gaussian with a full width at half maximum of 6.5 keV and a low-energy Compton tail. Due to the finite solid angle of the detector, also the  $\gamma$  quanta emitted at angles different from the flight angle  $\theta$  of  $^{12}\text{C}^*$  projectiles could be detected. As the  $\gamma$  energy varies with the emission angle  $\vartheta$ , the finite detection solid angle leads to an additional energy spread. The angular resolution function  $g(\vartheta)$  was determined by simulating the paths of  $\gamma$  rays from the target area to the detector with the Monte Carlo code GEANT4. Among the  $\gamma$  rays, only those absorbed in the detector were scored in the simulation, with the result that  $g(\vartheta)$  can be represented in a good approximation by a rectangular function with a width of  $20^\circ$ . The function  $g(\vartheta)$  was transformed from the angle coordinate into the function  $\tilde{g}(E_\gamma)$  in the  $\gamma$  energy coordinate using  $\tilde{g}(E_\gamma) = g[\vartheta(E_\gamma)] d\vartheta/dE_\gamma$ , where  $d\vartheta/dE_\gamma$  follows from Eq. (1). The final instrumental resolution function  $h(E_\gamma)$  is given by the convolution of the two functions  $f$  and  $\tilde{g}$ :

$h = \tilde{g} \otimes f$ . For discrete spectra, the deconvolution operation for the measured unattenuated spectrum  $y_u$  can be formulated as

$$(\tilde{\mathbf{G}} \times \mathbf{F}) \otimes \frac{dN_u}{dE_\gamma} = \mathbf{H} \otimes \frac{dN_u}{dE_\gamma} = y_u, \quad (8)$$

where  $\tilde{\mathbf{G}}$ ,  $\mathbf{F}$ , and  $\mathbf{H}$  are the matrices representing the functions  $\tilde{g}$ ,  $f$ , and  $h$  respectively. Equation (8) was solved iteratively by employing the gradient search method and using a reduced chi square of  $\chi_R^2 = 1$  as the stopping criterion of the iteration. The result is depicted in Fig. 3 showing the deconvolved and refolded spectrum in comparison to the measured spectrum. It is noteworthy that the slightly declining tail below 4450 keV arose due to not fully suppressed Compton scattering events of the  $\gamma$  photons emitted from  $^{12}\text{C}^*$  projectiles, which were considered by the low-energy tail of the detector response function.

The calculation of the start energy distribution of  $^{12}\text{C}^*$  projectiles according to Eq. (7) requires a unique relation between  $\theta$  and  $v_0$ . However, angular and energy straggling of the  $\alpha$  beam in the Ta foil can lead to a violation of this relation. Monte Carlo simulations were therefore carried out to estimate the energy and angular spread of the  $\alpha$  beam caused by the straggling processes. The results of the Monte Carlo simulations revealed that the uncertainty in  $dE_\gamma/dv_0$  arising due to these spreads is negligibly small compared to other uncertainties for  $\alpha$  beam energies higher than 11 MeV.

The start velocity distribution  $W(v_0)$  of  $^{12}\text{C}^*$  projectiles determined from the deconvolved unattenuated spectrum was used for the calculation of the attenuated spectrum  $dN_a/dE_\gamma$  according to Eq. (6). This calculated spectrum was then convolved with the instrumental resolution function  $h$  and compared with the measured, background subtracted spectrum  $y_a$  to determine the stopping power  $S(v)$  of water for  $^{12}\text{C}$  projectiles such that the following identity holds:

$$\psi \equiv \mathbf{H} \otimes \frac{dN_a}{dE_\gamma} = y_a. \quad (9)$$

Equation (9) is a Fredholm integral equation of the first kind, which was solved in this work numerically. For this purpose,  $S$  was represented as a function with four parameters, which was suggested by Paul and Schinner [15] for fitting the stopping power of solid targets for heavy ions from  $^3\text{Li}$  to  $^{18}\text{Ar}$ :

$$\frac{S(x)}{S_{\text{He}}(x)} = p_1 \left\{ p_2 + (1.01 - p_2) \left[ 1 - \exp \left( - \left( \frac{x + p_4 (\ln 2)^{1/d} - p_3}{p_4} \right)^d \right) \right] \right\}, \quad (10)$$

with  $d = 17.18 - 0.657 \times Z_1$  and  $x = \log_{10}(T/A_1)$ , where  $Z_1$  and  $A_1$  are the atomic and mass number of the projectile, respectively.  $S_{\text{He}}$  is the stopping power of water for helium ions which was calculated using the empirical formula of Ziegler [16]. The values of the parameters of the Ziegler formula were taken from ICRU Report No. 49 [17]. The values of the four dimensionless model parameters  $p_i$  were determined by means of weighted nonlinear regres-

sion analysis using the Levenberg-Marquardt algorithm [18]. Figure 4 shows the best fit to the experimental attenuated spectrum.

The uncertainty of the stopping power obtained by the above best fit was determined according to the Guide to the expression of uncertainty in measurement (GUM) [19]. For this purpose, the uncertainties  $u(p_i)$  of the best fit parameter values, which are mainly caused by random fluctuations in

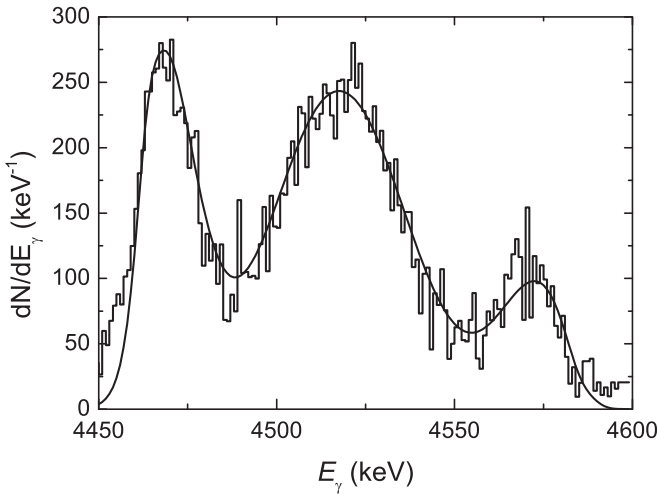


FIG. 4. Best fit (—) of Eq. (10) to the experimental, background subtracted attenuated spectrum (vertical steps).

the experimental spectra, were calculated from the covariance matrix  $\underline{C}$  according to  $u(p_i) = \sqrt{C_{ii}}$ . The covariance matrix is defined as  $\underline{C} = \chi_R^2 (\underline{J}^T \underline{W} \underline{J})^{-1}$ , where  $\underline{J}$  is the Jacobian matrix,  $\underline{W}$  is the diagonal weighting matrix with elements  $W_{ii} = 1/w_i^2$ , and  $\chi_R^2$  is the reduced weighted mean of the squared differences between the observed counts  $y_{ai}$  in the background-corrected attenuated spectrum and the fit function value  $\psi_i$ :

$$\chi_R^2 = \sum_i [(y_{ai} - \psi_i)/w_i]^2 / (n - m). \quad (11)$$

In Eq. (11),  $n$  and  $m$  are the number of data points and of the parameters, respectively. For the quantities  $w_i$  (that determine the elements of the weighting matrix), the statistical uncertainty of  $y_{ai}$  was used. Uncertainty propagation of the parameter uncertainties gives a combined contribution  $u_p$  to the standard uncertainty of the function  $S$  in Eq. (10) that is of type A and was calculated using

$$u_p^2 = \sum_{i=1}^4 \left( \frac{\partial S}{\partial p_i} \right)^2 u(p_i)^2. \quad (12)$$

The relative uncertainty  $u_p/S$  amounted to 8.6%. It should be noted that there is no uncertainty contribution related to the term  $S_{\text{He}}(x)$  in Eq. (10), as this is effectively a scaling constant used to make  $p_1$  a pure number. In principle, the product of the two quantities could be used as a fit parameter.

The second large uncertainty source was an energy shift of the attenuated spectrum relative to the unattenuated spectrum due to temporal drifts in the detection electronics. This energy shift can be corrected to a great part by adjusting the upper boundary of both spectra to the maximal possible  $\gamma$  energy, which can be determined from reaction kinematics and the Doppler formula, Eq. (1). The upper boundaries  $E_{\gamma, \text{max}}$  were obtained by linear extrapolations of the high-energy wings of the deconvolved attenuated and unattenuated spectra to the  $\gamma$  energy axis. The present statistics of the counts in the attenuated spectrum allowed the determination of  $E_{\gamma, \text{max}}$  to not better than  $u(E_{\gamma, \text{max}}) = 1.5$  keV. This value was obtained by observing the change of the upper boundaries when the

iterative deconvolution procedure was stopped at different  $\chi_R^2$  values varying within the 95% confidence interval. The uncertainty  $u(E_{\gamma, \text{max}}) = 1.5$  keV resulted in an additional relative type B uncertainty contribution of 5% in the stopping power. It is noteworthy that the influence of the angular resolution function of the detector on  $E_{\gamma, \text{max}}$  was disregarded because the  $\gamma$  emission angle at  $E_{\gamma, \text{max}}$  is  $0^\circ$  and the Doppler shift of the  $\gamma$  energy at  $0^\circ$  changes only slowly with the emission angle  $\vartheta$ .

The third major uncertainty source is the lifetime of  $^{12}\text{C}^*$  nuclei, which has a relative type B uncertainty of  $u_l^r = 5.7\%$  that propagates with a factor of unity into the uncertainty of  $S$ . All other sources of uncertainty added only negligibly small contributions to the relative uncertainty of  $S$ . It should be noted that the uncertainty arising from the inaccuracy of the background subtraction of the attenuated spectrum was also very small as the background was nearly constant. Furthermore, this uncertainty was included in the uncertainty contribution from the fit parameters. As mentioned above, the background in the unattenuated spectrum was negligibly small. The overall relative uncertainty, obtained as the square root of the sum of squared individual uncertainties, amounts to 11.4%. The individual dominant uncertainty sources are summarized in Table I

## V. RESULTS AND DISCUSSION

The stopping power of water for  $^{12}\text{C}$  projectiles corresponding to the best fit shown in Fig. 4 is displayed in Fig. 5 in comparison to other semiempirical and theoretical data. The best agreement was found between the results of this work and the data recommended in the Errata and Addenda for ICRU Report No. 73 [20]. They concur not only in the magnitude but also in the energy dependence. It is noteworthy that the above ICRU data were calculated using the PASS code [21] and an  $I$  value of 78 eV, which is considerably higher than the value of 67.2 eV given in the original ICRU Report No. 73 [22].

In the year 2014, the ICRU revised the data for the stopping power of liquid water for carbon ions [23] in the intermediate and low energy region. In the new recommendation given in ICRU Report No. 90, the PASS code was replaced by the MSTAR code [24], which was devised to provide semiempirical data for the electronic stopping power of solids for heavy ions. The use of the MSTAR code in place of the PASS code was motivated by the fact that the former code better reproduced the experimental data for the stopping power of water for Li ions [25]. It can be seen from Fig. 5 that the present results also agree well with the new recommended data of ICRU Report No. 90 above 3 MeV within the experimental uncertainties. Below 3 MeV, however, the values given in Errata and Addenda for ICRU Report No. 73 better reproduce the results of this work.

It is remarkable that SRIM 2013 [26] predicts noticeably higher values than other codes and the present experiment for kinetic energies higher than 3 MeV. At  $T = 4$  MeV, the difference between the result of this work and the SRIM data amounts to about 16%. The SRIM code calculates the stopping power of compound materials based on the so-called core and bond approach (CAB) [27]. In this approach, the stopping

TABLE I. Summary of the individual uncertainties contributing to the overall uncertainty of the present results of 11.4%.

Uncertainty	$u_p$	$u_b$	$u_l$
Source	Type A uncertainties of the fit parameters caused by random fluctuations in the measured $\gamma$ energy spectra	Type B uncertainties caused by the inaccuracy in determining the upper boundaries $E_{\gamma,\max}$ of the measured $\gamma$ energy spectra	Type B uncertainty arising due to the uncertainty of the lifetime of the first excited state of $^{12}\text{C}^*$
Determination procedure	1. covariance matrix $\underline{C}$ for the fit parameters $p_i$ ;  2. uncertainties $u(p_i)$ of the fit parameters determined from $\underline{C}$ ; 3. $u_p$ using Eq. (10)	1. $u(E_{\gamma,\max})$ determined from the change of $E_{\gamma,\max}$ when the deconvolution procedure was stopped at different $\chi^2_R$ within the confidence interval of 95%; 2. solution of Eq. (9) with an attenuated spectrum shifted by $u(E_{\gamma,\max})$ ; 3. $u_b$ given by the difference of $S$ for shifted and nonshifted spectrum	Ref. [13].
Relative value	8.6 %	5.0%	5.7%

power is represented as a sum of the contribution of core and binding electrons, where the former is computed by means of the Bragg additivity rule [28] and the latter was determined by analyzing experimental stopping power of a variety of compounds for H, He, and Li ions. Here, inaccuracies may arise when extrapolating the contribution of binding electrons from the lighter to carbon ions.

In contrast to SRIM and the MSTAR code, the CASP code [29] calculates ion stopping cross sections of molecules an-

alytically using electron density distribution and oscillator strengths of the atomic constituents. A special focus is given to the influence of screening of projectiles carrying electron on energy loss. In this work, the stopping cross section of water molecules for carbon ions was theoretically computed using CASP code with the so-called unitary convolution approximation [30] and an  $I$  value of 78 eV. The calculation was performed in the charge state scan mode where the stopping cross section is obtained as the weighted sum of the stopping cross sections associated with each charge state of the projectile. It can be seen from Fig. 5 that the predictions of the CASP code tend to be somewhat lower than those of other codes. It can be, however, stated that within the experimental uncertainties, the present results comply with the theoretical values obtained using the CASP code when including the contribution of charge changing processes to ion stopping.

When disregarding projectile screening, the stopping power of a given medium scales in the first approximation with the square of effective projectile charge [31]. The concept of point effective charge is, however, applicable only to a limited extent for heavy ions in the intermediate and low-energy region. In this energy region, the screening of the projectile, which varies with the impact parameter, plays an important role in energy loss processes [32]. The CASP code accounts for the dependence of projectile screening on impact parameter by calculating the energy loss as function of the impact parameter. Bearing this in mind, it was assumed that the CASP code allows accurate determination of the dependence of stopping power on projectile charge.

Most of the experimental investigations with respect to the stopping power of water have been carried out for  $\alpha$  particles [2–7], primarily because  $\alpha$  particles are easily available from radioisotopes and no accelerator is required for their production. As there exists no experimental data for the stopping

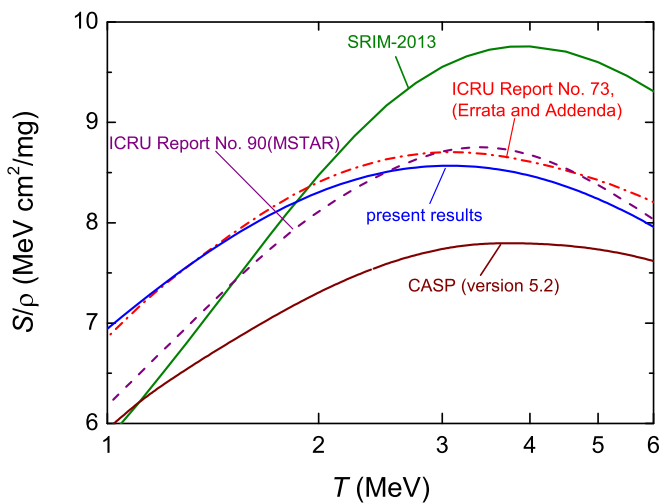


FIG. 5. Present results for the mass stopping power of water for carbon ions in comparison to semiempirical and theoretical data. The theoretical data computed using the CASP code include the contribution of charge exchange processes to energy loss. The calculation was performed in the charge state scan mode using the UCA approximation [30].

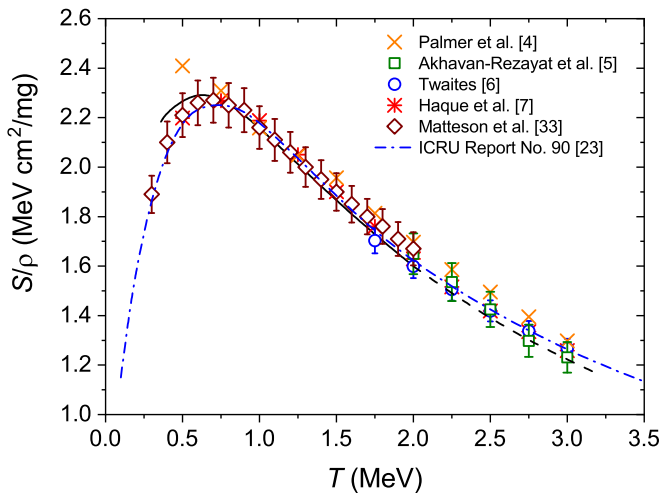


FIG. 6. Comparison of the mass stopping power of water for  $\alpha$  particles measured by different groups. The solid line represents the data scaled from the present results for carbon ions using a scaling factor, which was calculated by means of the CASP code. Above  $T > 2.0$  MeV, these data are depicted by a dashed line to indicate that they are obtained using the extrapolated data based on Eq. (10).

power of water for carbon ions reported by other groups, the present results were intercompared to the measured data for  $\alpha$  particles. For this purpose, the ratio of the stopping power of water for  $\alpha$  particles to that for carbon ions at a given projectile velocity was calculated using the CASP code. This ratio was then multiplied with the results of this work to obtain the stopping power of water for  $\alpha$  particles.

Figure 6 shows the stopping power of water for  $\alpha$  particles obtained in the way described above in comparison to published experimental data. The results for  $T > 2$  MeV are depicted as a dashed line to indicate that they are extrapolated values based on Eq. (10). It can be seen from Fig. 6 that the present results agree with the experimental data of other groups within the experimental uncertainties. A very good agreement was found between the values obtained by the extrapolation of the present results and the data of Akhavan-Rezayat and Palmer [5] in the energy region above 2 MeV. It should be mentioned that the data of Matteson *et al.* [33] were measured with H<sub>2</sub>O ice. As is further evident from Fig. 6, the data for  $\alpha$  particles recently recommended in ICRU Report No. 90 [23] based on an  $I$  value of 78 eV are fairly well reproduced by the present results above 1 MeV.

## VI. CONCLUSIONS

The stopping power of liquid water was remeasured for carbon ions in the energy range between 1 and 6 MeV using the IDSA method [12]. In this experiment, the background in the attenuated spectrum was considerably reduced by employing a BGO Compton shield. Furthermore, the unattenuated spectrum was measured at the same  $\alpha$  beam energy as in the case of the attenuated spectrum, which enabled accurate determination of the start velocity distribution of  $^{12}\text{C}^*$  projectiles.

Among several semiempirical and theoretical data, the best agreement was found between the data recommended in the Errata and Addenda of ICRU Report No. 73 [20] and the results of this work. The recent recommendation given in ICRU Report No. 90 [23] is somewhat lower than the present results for  $T < 3$  MeV while the SRIM 2013 code [26] seems to overestimate the stopping power of water for carbon ions in the energy region around the stopping power maximum.

The semiexperimental stopping power of water for  $\alpha$  particles obtained by scaling of the present results for carbon ions agrees surprisingly well with the literature values [2–7,33] throughout the whole investigated energy range within the experimental uncertainties. The good agreement with the ICRU values [20,23] above the stopping power maximum underpins the  $I$  value of 78 eV for water.

The overall uncertainty of about 11% is still too high for the purpose of precise treatment planning in radiotherapy. This uncertainty is mainly caused by the statistical uncertainty in the attenuated spectrum. A longer measurement with the present experimental setup and more accurate determination of the lifetime of the first excited state in  $^{12}\text{C}^*$  could reduce the uncertainty to below 5%.

## ACKNOWLEDGMENTS

This research was funded by Deutsche Forschungsgemeinschaft (DFG, German Research Foundation) under Project No. BA 5371/3-1. The authors gratefully thank the staff of the Institute for Nuclear Physics of University of Cologne, especially C. Müller-Gatermann and C. Fransen, for their technical and scientific assistance. The support by the group of H. Hofsäss at the University of Göttingen in producing a stable carbon coating of tantalum foils is also gratefully acknowledged. The authors extend their thanks to H. Nittmann, S. Otto, and A. Pausewang for their assistance in preparing and conducting the experiment.

[1] K. Philipp, *Z. Phys.* **17**, 23 (1923).  
 [2] G. Aniansson, *Phys. Rev.* **98**, 300 (1955).  
 [3] M. McNally, *Proc. R. Soc. London, Ser. A* **237**, 28 (1956).  
 [4] R. B. J. Palmer and A. Akhavan-Rezayat, *J. Phys. D: Appl. Phys.* **11**, 605 (1978).  
 [5] A. Akhavan-Rezayat and R. B. J. Palmer, *J. Phys. E: Sci. Instrum.* **13**, 877 (1980).  
 [6] D. I. Twaites, *Phys. Med. Biol.* **26**, 71 (1981).  
 [7] A. K. M. M. Haque, A. Mohammadi, and H. Nikjoo, *Radiat. Protect. Dosim.* **13**, 71 (1985).

[8] M. Shimizu, M. Kaneda, T. Hayakawa, H. Tsuchida, and A. Itoh, *Nucl. Instrum. Methods Phys. Res. B* **267**, 2667 (2009).  
 [9] M. Shimizu, T. Hayakawa, M. Kaneda, H. Tsuchida, and A. Itoh, *Vacuum* **84**, 1002 (2010).  
 [10] T. Siiskonen, H. Kettunen, K. Peräjärvi, A. Javanainen, M. Rossi, W. H. Trzaska, J. Turunen, and A. Virtanen, *Phys. Med. Biol.* **56**, 2367 (2011).  
 [11] J. M. Rahm, W. Y. Baek, H. Rabus, and H. Hofsäss, *Phys. Med. Biol.* **59**, 3683 (2014).

- [12] W. Neuwirth, U. Hauser, and E. Kühn, *Z. Phys.* **220**, 241 (1969).
- [13] F. Ajzenberg-Selove and C. L. Busch, *Nucl. Phys. A* **336**, 1 (1980).
- [14] G. E. Mitchell, E. B. Carter, and R. H. Davis, *Phys. Rev.* **133**, B1434 (1964).
- [15] H. Paul and A. Schinner, *Nucl. Instrum. Methods Phys. Res. B* **195**, 166 (2002).
- [16] J. F. Ziegler, *Helium: Stopping Powers and Ranges in All Elemental Matter*, The Stopping and Ranges of Ions in Matter Vol. 4 (Pergamon, Elmsford, NY, 1977).
- [17] International Commission on Radiation Units and Measurements, *Stopping Powers and Ranges for Protons and Alpha Particles*, ICRU Report No. 49 (ICRU, Bethesda, Maryland, 1993).
- [18] R. C. Aster, B. Borchers, and C. H. Thurber, *Parameter Estimation and Inverse Problems*, 2nd ed. (Academic, Oxford, 2013).
- [19] *International Organization for Standardization* Guide to the Expression of Uncertainty in Measurement, 1st ed (Geneva, 1993).
- [20] P. Sigmund, A. Schinner, and H. Paul, Errata and Addenda for ICRU Report No. 73, 2009.
- [21] P. Sigmund and A. Schinner, *Nucl. Instrum. Methods Phys. Res. B* **195**, 64 (2002).
- [22] *International Commission on Radiation Units and Measurements*, ICRU Report No. 73, J. ICRU5 No. 1 (Oxford University Press, Oxford, 2005).
- [23] *International Commission on Radiation Units and Measurements*, ICRU Report No. 90, J. ICRU14, No. 1 (Oxford University Press, Oxford, 2014).
- [24] H. Paul and A. Schinner, *At. Data Nucl. Data Tables* **85**, 377 (2003).
- [25] W. Neuwirth, W. Pietsch, K. Richter, and U. Hauser, *Z. Phys.* **275**, 209 (1975).
- [26] J. F. Ziegler, M. D. Ziegler, and J. P. Biersack, *Nucl. Instrum. Methods Phys. Res. B* **268**, 1818 (2010).
- [27] G. Both, R. Krotz, K. Lohmer, and W. Neuwirth, *Phys. Rev. A* **28**, 3212 (1983).
- [28] W.H. Bragg and R. Kleeman, *Philos. Mag.* **10**, 318 (1905).
- [29] G. Schiwietz and P. L. Grande, *Phys. Rev. A* **84**, 052703 (2011).
- [30] P. L. Grande and G. Schiwietz, *Nucl. Instrum. Methods Phys. Res. B* **195**, 55 (2002).
- [31] W. Brandt and M. Kitagawa, *Phys. Rev. B* **25**, 5631 (1982).
- [32] G. M. Azevedo, P. L. Grande, and G. Schiwietz, *Nucl. Instrum. Methods Phys. Res. B* **164-165**, 203 (2000).
- [33] S. Matteson, D. Powers, and E. K. L. Chau, *Phys. Rev. A* **15**, 856 (1977).